

Influence of Long-Term CaO Storage Conditions on the Calcium Looping Thermochemical Reactivity

Nabil Amghar, Antonio Perejón,* Carlos Ortiz, Luis A. Pérez Maqueda,* and Pedro E. Sánchez-Jiménez*




Cite This: *Energy Fuels* 2023, 37, 16904–16914



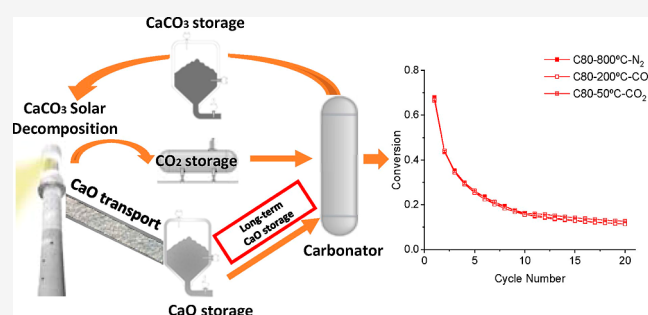
Read Online

ACCESS |

 Metrics & More

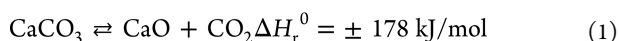
 Article Recommendations

ABSTRACT: Long-term storage capability is often claimed as one of the distinct advantages of the calcium looping process as a potential thermochemical energy storage system for integration into solar power plants. However, the influence of storage conditions on the looping performance has seldom been evaluated experimentally. The storage conditions must be carefully considered as any potential carbonation at the CaO storage tank would reduce the energy released during the subsequent carbonation, thereby penalizing the round-trip efficiency. From lab-scale to conceptual process engineering, this work considers the effects of storing solids at low temperatures (50–200 °C) in a CO₂ atmosphere or at high temperatures (800 °C) in N₂. Experimental results show that carbonation at temperatures below 200 °C is limited; thus, the solids could be stored during long times even in CO₂. It is also demonstrated at the lab scale that the multicycle performance is not substantially altered by storing the solids at low temperatures (under CO₂) or high temperatures (N₂ atmosphere). From an overall process perspective, keeping solids at high temperatures leads to easier heat integration, a better plant efficiency (+2–4%), and a significantly higher energy density (+40–62%) than considering low-temperature storage. The smooth difference in the overall plant efficiency with the temperature suggests a proper long-term energy storage performance if adequate energy integration is carried out.



INTRODUCTION

The calcium looping (CaL) process has been intensely investigated in the last years as a promising system for thermochemical energy storage (TCES).^{1–4} It is based on the reversible reaction between CO₂ and CaO to form CaCO₃ (eq 1)



The use of CaL as a mid to high-temperature carbon capture and storage technology is currently at the technology readiness level (TRL) 7.^{5,6} As a TCES system, CaL displays several advantages, such as high energy density, nontoxicity, and the wide availability and affordability of the potential raw materials, which include Ca-containing minerals, rocks, and even industrial wastes.^{2,7–10}

TCES based on CaL has been typically considered to be integrated into concentrating solar power (CSP) due to the compatible charge and discharge temperatures.^{11,12} Solar radiation drives the endothermic decomposition of CaCO₃ into CaO and CO₂ in a solar reactor.^{3,13} The reaction products are separately conducted to storage reservoirs and then brought back together in the carbonator reactor on demand for energy production. The heat released in the reverse

exothermic reaction is exploited in a power cycle (i.e., CO₂-closed Brayton cycle) to produce electricity.^{14,15} The equilibrium temperature in a CO₂ atmosphere at 1 bar is ~895 °C.¹⁶ Consequently, for achieving fast calcination in CO₂, the reaction temperature has to be maintained above ~950 °C.^{17,18} The carbonation reaction is normally proposed at ~800–850 °C to ensure a rapid reaction and high thermoelectric efficiency.^{14,19,20} High temperature and CO₂-rich environments substantially promote the grain growth and sintering of CaO particles, which, consequently, speed up the deactivation of CaO.^{18,21–23} Thus, the calcination stage is frequently carried out under an inert gas or at reduced pressure, which allows the reduction of the minimum required temperature to 750 °C.^{24–26}

A literature review of recent studies on the CaL system shows a profound interest in sorbent properties, reactor design

Received: July 18, 2023

Revised: October 4, 2023

Published: October 20, 2023



and operation, process integration, and economic analyses.^{27–30} Lately, there has been progress in the design of more efficient and potentially cost-effective plant schemes. Multiple options have been contemplated, such as fuel consumption and equipment size reduction,^{31,32} improvement in heat transfer from hot calcination products to colder carbonation sorbents,^{33,34} reactivation of the sorbent,³⁵ and integration with solar technologies.^{13,36–38}

One of the key advantages of CaL as a TCES system is the possibility of long-term energy storage. Current state-of-the-art thermal storage (TES) technologies are mainly based on molten salts. In this case, the need to trace the system to maintain temperatures over 200 °C to avoid the solidification of the molten salts entails a substantial increase in costs.^{27,39} Many process schemes in the literature consider either high temperature or low temperature solids storage for CaL integration.^{27,40–42} However, none of the studies published in the literature have yet considered the influence of the storage conditions on the CaO reactivity, and only a few studies have directly compared the effect of storing the solids at high or low temperatures.^{43–46} Understanding the storage stage influence is crucial to optimize the whole process. An excessively high storage temperature of the reactants might deteriorate the CaO reactivity due to sintering.^{18,47} The atmosphere is also relevant because of the high reactivity of CaO with H₂O and CO₂. Thus, even small contents of moisture and CO₂ might partially convert CaO into Ca(OH)₂ or CaCO₃ during the storage period, thereby incurring undesired energy release during the storage step.⁴⁸

The present work explores the impact of the storage conditions of the reactants on the multicycle activity of CaO for TCES. While previous research has evaluated the influence of using different storage temperatures for the CaO silos, there are no studies considering the influence on CaO multicycle performance. Thus, the performance of limestone has been evaluated when a storage step is inserted between the calcination and carbonation cycles. Three different storage temperatures have been explored; 50 and 200 °C under CO₂ and 800 °C under N₂. This work also contemplates the influence of critical parameters such as temperature, atmosphere, particle size, and time. Finally, the impact of the storage temperature over the round trip efficiency is also assessed from a process engineering perspective.

MATERIALS AND METHODS

Materials. Limestone was provided by KSL Staubtechnik GmbH from the standard Eskal series. According to the supplier, the limestone has 99.1% content in CaCO₃ but also contains as impurities 0.45% MgO, 0.25% SiO₂, 0.1% Al₂O₃, and 0.04% Fe₂O₃. Samples with two well-defined particle sizes were used: 80 and 150 μm. These particle sizes were selected considering that particles below 50 μm cannot be fluidized in the proposed practical application due to their cohesiveness.^{49–51} The samples are referred to hereafter as C80 and C150, respectively.

Particle size distribution (PSD) data are listed in Table 1, while the frequency distributions of the particle sizes for the samples are plotted in Figure 1. As can be seen, the samples present a narrow PSD.

EXPERIMENTAL METHODS

The multicycle activity was studied in a thermogravimetric analyzer Q5000 developed by TA Instruments, equipped with a high sensitivity balance (<0.1 μm). This instrument allows for high heating and cooling rates (~300 °C/min) from room temperature to 1000 °C, using infrared halogen lamps that heat the silicon carbide furnace

Table 1. PSD Parameters of the Two Limestone Samples^a

sample	PSD data (μm)		
	Dv(10)	Dv(50)	Dv(90)
C80	1.60	74.91	133.47
C150	113.11	133.60	157.24

^aDv(10), Dv(50), and Dv(90) indicate the percentiles, meaning that 10, 50, and 90% of the sample is smaller than the given size, respectively.

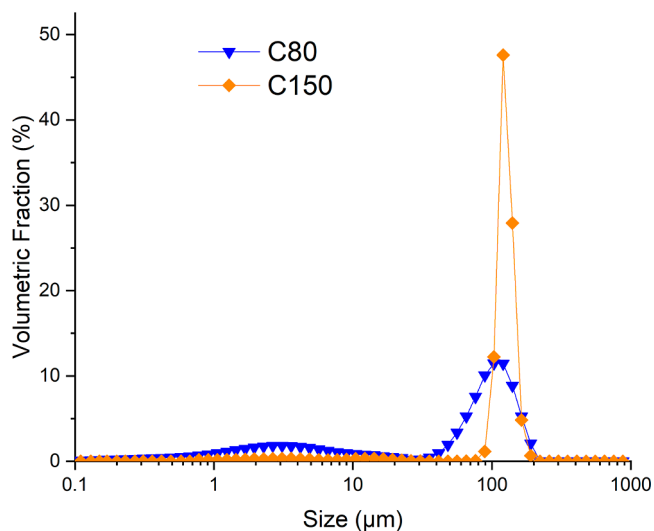


Figure 1. PSD data measured for C80 and C150.

where the sample is placed. These high heating rates are necessary to simulate realistic Ca-Looping conditions in which the material undergoes calcination and carbonation under different atmospheres and temperatures.

Two experimental schemes were used in this work. The first one comprises an initial heating step to a calcination temperature of 950 °C in a CO₂ atmosphere. The calcination temperature is maintained for 3 min. Then, the atmosphere is switched to N₂, and purged for 5 min to ensure the complete removal of CO₂ from the system. This is done to avoid carbonation while cooling to the storage step in order to correctly assess the results and discriminate the influence of CO₂ in the storage step. The system is cooled to the desired storage temperature (200 and 50 °C). Once the storage temperature is achieved, the atmosphere is again switched to CO₂ and maintained for the planned storage time. To evaluate the influence of storage on subsequent carbonation stages, the sample is heated in nitrogen to a carbonation temperature of 800 °C at 300 °C/min, when the atmosphere is changed to CO₂. For example, Figure 2 shows a scheme of the test involving storage in CO₂ at 50 °C.

The second scheme represents a CSP CaL process scheme in which solids are stored at high temperatures to simplify the reactors' thermal integration.¹⁵ The storage step is introduced at high temperatures in a N₂ atmosphere between the calcination and carbonation stages. The calcination is performed at 950 °C in CO₂, and then, the atmosphere is switched to N₂. The system is then cooled to a storage temperature (800 °C), which lasts 1 h in this atmosphere. Then, to proceed with the multicycle tests, the atmosphere is changed to CO₂, and the carbonation is triggered at 850 °C during 5 min. Table 2 summarizes the experimental conditions for the evaluation of the multicycle performance used in this work.

The PSD was measured by laser diffraction using a Mastersizer 2000 from Malvern. The samples were sonicated for 30 min and dispersed in distilled water to avoid aggregation.

CaO Conversion and Residual CaO Conversion. The conversion of CaO to CaCO₃ is the main parameter used in this

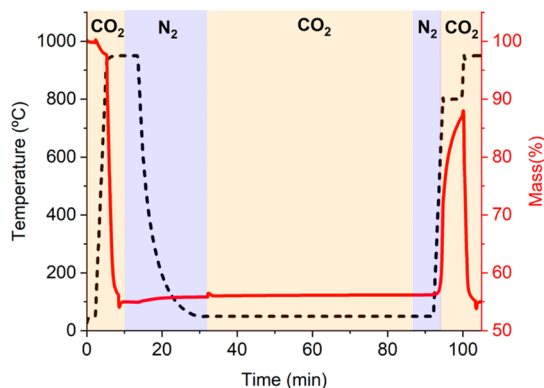


Figure 2. Schematic diagram of the experimental procedure for evaluating storage tests. Blue and yellow indicate which experiment segments were carried out in N_2 or CO_2 atmospheres, respectively.

work to evaluate the multicycle performance of the samples. The total CaO conversion ($X_{T,N}$) in each cycle is defined as the sum of the CaO conversion during storage (X_{sto}) (which is undesirable since the heat is not being released to the power cycle) and the conversion in the subsequent carbonation stage ($X_{CaO,N}$)

$$X_{T,N} = X_{sto,N} + X_{CaO,N} \quad (2)$$

Moreover, $X_{T,N}$ may be expressed as

$$X_{T,N} = \frac{m_{T,N} - m_N}{m_N} \cdot \frac{W_{CaO}}{W_{CO_2}} \quad (3)$$

where $m_{T,N}$ is the total sample mass after the storage step and the subsequent carbonation stage and m_N is the sample mass after calcination (before the storage starts). W_{CaO} and W_{CO_2} are the molar masses of CaO and CO_2 , respectively.

The undesired conversion of CaO that would take place during the storage step is

$$X_{sto,N} = \frac{m_{sto,N} - m_N}{m_N} \cdot \frac{W_{CaO}}{W_{CO_2}} \quad (4)$$

where m_{sto} is the sample mass after the storage step at the N th-cycle. X_{sto} considers the nondesired reaction of CaO with CO_2 during storage. The heat released during this step would be wasted.

From the above equations, the CaO conversion in the carbonation stage of the cycles can be obtained once the values of $X_{T,N}$ and $X_{sto,N}$ are calculated

$$X_{CaO,N} = X_{T,N} - X_{sto,N} \quad (5)$$

Energy Storage Density of the Calcined Material. The energy storage density (in GJ/m^3) of the calcined materials can be quantified from the energy density per mass

$$D_m = \frac{m_{CO_2} \times \Delta H_R}{m_N} \quad (6)$$

Here, m_{CO_2} is the CO_2 uptake during carbonation, computed from the CaO conversion data, ΔH_R is the enthalpy of the reaction per kg of CO_2 (4045.5 kJ/kg CO_2), and m_N is the sample mass after calcination. The energy storage density is then calculated from eq 8

$$D_v = D_m \times \rho \quad (7)$$

where ρ is the density of the calcined material, assuming a porosity of 50% (for CaO, it results in a density of 1670 kg/m^3). Given this value, the maximum theoretical volumetric energy density for CaO would be 3.7 GJ/m^3 .

RESULTS AND DISCUSSION

Effect of Storage in CO_2 at Different Temperatures.

Optimum storage conditions for CaO are essential to ensure a proper plant's overall performance. The storage temperature imposes rules for thermal energy integration of the reactors. Besides, the material's reactivity during the storage step should also be considered an essential parameter that could reduce the available energy released into the power cycle.

Figure 3 shows the behavior during storage of CaO derived from the decomposition of C80 limestone particles at different

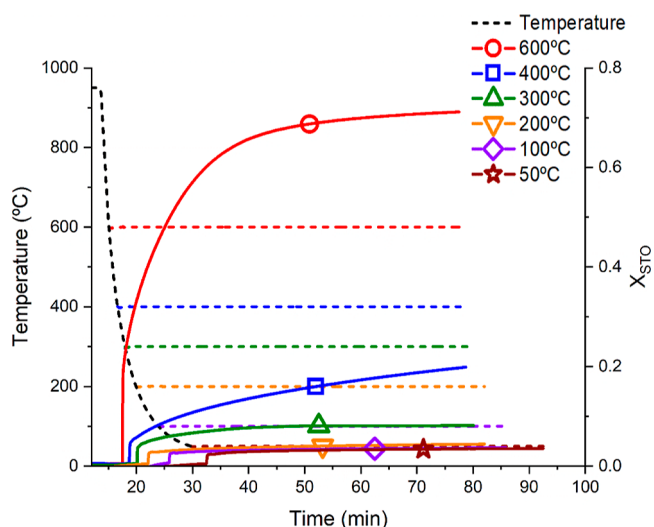


Figure 3. Time evolution of the storage conversion for calcined C80 samples, maintained in a CO_2 atmosphere at different temperatures.

temperatures under a CO_2 atmosphere. Thus, in these experiments, a freshly calcined sample is rapidly cooled down to a set storage temperature. Only when the desired temperature is reached, CO_2 is injected into the system (as described in Figure 2). Almost immediately after CO_2 injection, the sample mass increases due to the carbonation. Two carbonation stages are evident; a very fast reaction-controlled stage followed by a slower, diffusion-controlled

Table 2. Experimental Conditions for the Different Calcination/Carbonation Tests Carried Out in This Work

test	calcination			carbonation			storage		
	$T, ^\circ C$	$t, \text{ min}$	gas	$T, ^\circ C$	$t, \text{ min}$	gGas	$T, ^\circ C$	$t, \text{ min}$	gas
C80-50 °C- CO_2	950	5	CO_2	800	5	CO_2	50	60	CO_2
C80-200 °C- CO_2	950	5	CO_2	800	5	CO_2	200	60	CO_2
C80-800 °C- CO_2	950	5	CO_2	800	5	CO_2	800	60	N_2
C150-50 °C- CO_2	950	5	CO_2	800	5	CO_2	50	60	CO_2
C150-200 °C- CO_2	950	5	CO_2	800	5	CO_2	200	60	CO_2
C150-800 °C- CO_2	950	5	CO_2	800	5	CO_2	800	60	N_2

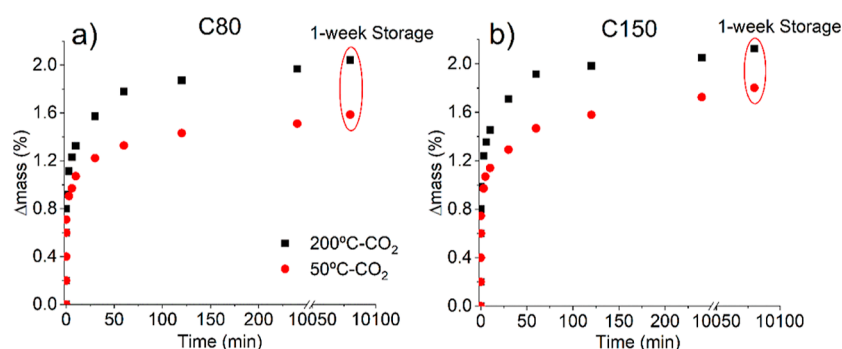


Figure 4. Mass percentage gains as a function of time for samples tested at 50 and 200 °C in CO₂. (a) C80 and (b) C150. Legend is shared for both graphics and represents the temperature of the storage step. The red ellipse highlights the value for 1 week storage.

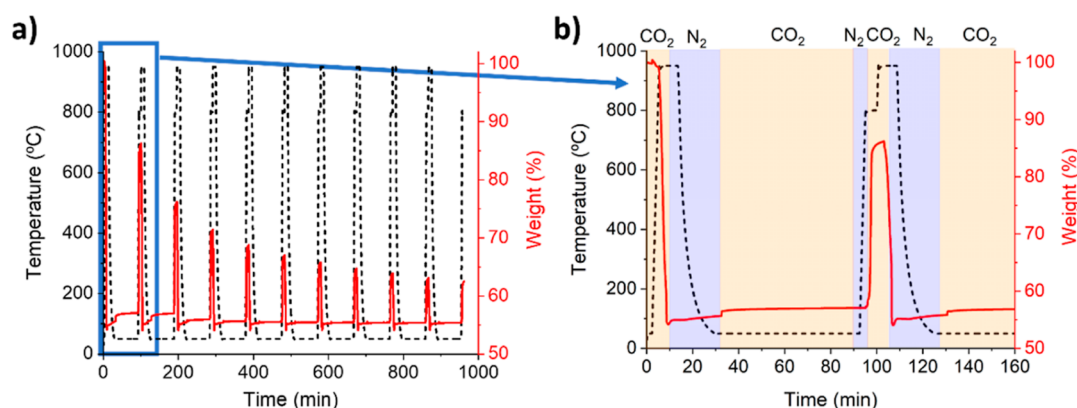


Figure 5. (a) Time evolution of temperature and sample mass (C80 sample) recorded in the thermogravimetric analysis during multicycle calcination/carbonation tests using a 60 min storage step at 50 °C. (b) Close-up view of the first cycle. Calcination and carbonation were carried out in a CO₂ atmosphere for 5 min at 950 and 800 °C, respectively. Blue and yellow highlight the segments under N₂ or CO₂ atmospheres, respectively.

carbonation stage.^{21,52,53} The higher the temperature, the more significant the fraction of CaO that converts into CaCO₃ during the fast carbonation stage. Likewise, diffusion-controlled carbonation is equally promoted at higher temperature. It is evident from Figure 3 that storing the solids under pure CO₂ at 600 and 400 °C is undoubtedly detrimental as the carbonation reaction is kinetically very favored at these temperatures. A storage temperature of 600 °C approaches the conditions used in CO₂ capture applications, where carbonation occurs at 650 °C under a less rich CO₂ atmosphere (~10–15% vol.).^{54,55} On the other hand, it appears that at temperatures below 200 °C, the carbonation results in essentially similar values of CaO conversion ($X_{\text{sto}} = 0.04$). Thus, cooling the CaO all the way down to room temperature might not be necessary to preserve the reactivity of the material for subsequent carbonation cycles.

Consequently, storage at temperatures higher than 200 °C must be avoided if the material is stored under a pure CO₂ atmosphere. The storage temperature of 200 °C can be used as a proper comparison with the current molten salt storage temperature,⁵⁶ while the storage temperature at 50 °C is a reference for room temperature storage. Remarkably, in the case of CaO particles, there are no significant issues if particles are cooled from 200 °C, so there is no critical process limitation as in the case of molten salts.

Effect of Storage Time in CO₂. The storage of the reaction products is expected to last for at least some hours (if not days, as potentially occurred in TCES systems). Consequently, the time that CaO can be stored without

activity loss in subsequent cycles is relevant to the overall process efficiency. Figure 4 shows the time evolution of the mass percentage gained during the storage step in CO₂ for C80 and C150 limestone particles. For this study, an experiment similar to that presented in Figure 2 was performed but with extended storage times. Two different storage temperatures were compared: 50 and 200 °C.

As seen in Figure 4, the main part of the overall conversion occurs within the first 30–50 min. Moreover, about half of the total mass gain occurs during the first 6 s after CO₂ is injected, regardless of particle size. Noticeably, the observed behavior is similar to the carbonation profiles at higher temperatures: a fast controlled reaction phase lasts only a few seconds, followed by a slower diffusion-controlled reaction phase.^{21,52,53} It can be inferred from the experiments in Figure 4 that long-term storage is feasible as the loss of active material is very small due to the limited fast controlled reaction phase at 50 and 200 °C and the very slow diffusion-controlled carbonation kinetics. Note that after 1 week, the mass percentage gained is still lower than 2.2%, indicating that long-term storage at 50 and 200 °C is feasible even in a CO₂ atmosphere. Considering these results, a storage time of 60 min was used in the subsequent experiments since higher solids storage times would not substantially alter the obtained results.

Effect of the Storage Step on the Multicycle Performance. Figure 5a displays the time evolution of the mass along multiple calcination–carbonation cycles recorded for C80 particles. The multicycle scheme includes a 60 min

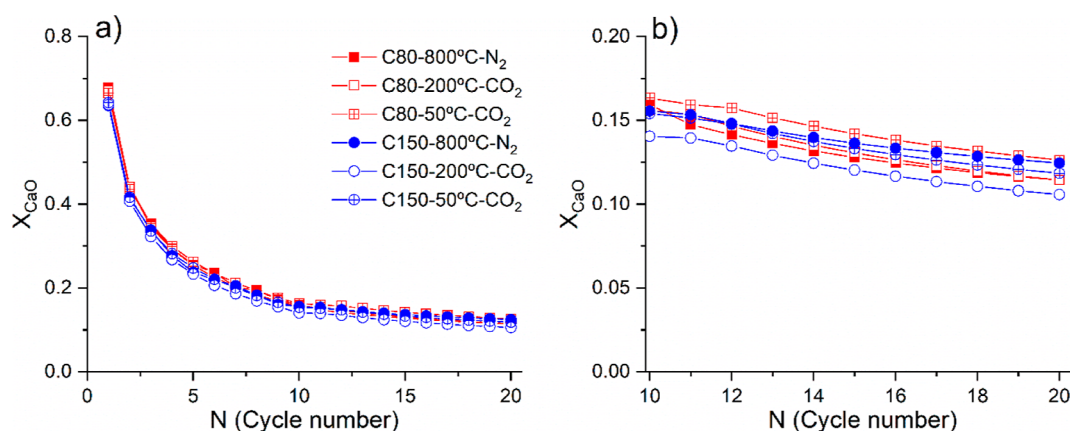


Figure 6. (a) Multicycle evolution of the CaO conversion, calculated from eqs 4 and 5, for C80 and C150. (b) Close-up of the last 10 cycles for C80 and C150. Legend is shared for both graphs. Unfilled symbols represent samples submitted to the 200 °C storage step, and cross-filled symbols represent samples submitted to the 50 °C storage step. Solid symbols represent CaO conversion when a storage step at a high temperature (800 °C) in N₂ is considered (5 min calcination and carbonation at 950 and 800 °C, respectively).

storage step at 50 °C after each calcination stage. Figure 5b corresponds to a close view of the first cycle; it shows that the calcination temperature of 950 °C ensures a rapid conversion of CaCO₃ into CaO. A progressive deactivation of CaO toward carbonation as the number of cycles increases is evident in Figure 5a due to sintering, which is further promoted in the CO₂-rich atmosphere because of the higher temperature required for calcination.^{18,23}

Figure 6 compares the multicycle performance in terms of CaO conversion (X_{CaO}) for C80 and C150. CaO conversions are calculated from the thermogravimetry experiments according to eq 5. Three different storage conditions were explored: (i) 50 °C in CO₂, (ii) 200 °C in CO₂, and (iii) 800 °C in N₂. It can be readily concluded from the plots that the overall behavior of the materials does not depend on particle size in the range 80–150 μm. In all three operating conditions studied, the CaO conversions dropped from about 0.65–0.70 in the first cycle down to about 0.17 after 20 calcination and carbonation cycles. Table 3 lists the CaO conversion attained

Table 3. Values of CaO Conversion for the 1st ($X_{\text{CaO},1}$) and 20th ($X_{\text{CaO},20}$) Cycles

sample	storage 200 °C (CO ₂)		storage 50 °C (CO ₂)		storage 800 °C(N ₂)	
	$X_{\text{CaO},1}$	$X_{\text{CaO},20}$	$X_{\text{CaO},1}$	$X_{\text{CaO},20}$	$X_{\text{CaO},1}$	$X_{\text{CaO},20}$
C80	0.670	0.114	0.665	0.126	0.678	0.114
C150	0.637	0.106	0.642	0.118	0.635	0.124

at the 1st and 20th cycles for C80 and C150 under the different experimental conditions. The conversion values obtained agree with previous reports for similar particle sizes.⁵⁷ These results demonstrate that the samples present a similar behavior regardless of the storage conditions implemented.

Figure 7 compares the results obtained in terms of volumetric energy density, calculated as described in eqs 6 and 7. Red bars correspond to the values calculated using the CaO conversion during the carbonation stage, X_{CaO} , that is, the energy that can be recovered. On the other hand, blue bars account for the fraction of the energy density wasted during the storage step. Both storage conditions in CO₂ (200 and 50 °C) yield good results in terms of the capability to preserve the

CaO reactivity. As the reactivity of the material decreases with the subsequent cycles, so does the fraction of material that reacts during the storage step. Thus, while non-negligible at a low cycle number, after 5 cycles, the CaO becomes unreactive at low temperatures, and the energy lost during storage becomes negligible. Obviously, in the experiments testing storage in N₂, there is no energy wasted during storage, as this is implemented in an inert atmosphere.

Table 4 includes the accumulated energy density, calculated as the sum of the energy density (D_v) of each of the 20 calcination/carbonation cycles performed. The energy density values obtained are roughly similar for C80 particles. On the other hand, C150 particles exhibit worse long-term performance when stored in CO₂ at 200 °C.

Considerations on the Industrial-Scale TCES Process Integration. This section broadens the focus of the study to assess how a given storage condition can affect the overall performance (net solar-to-electricity and energy density) of the thermochemical storage system on an industrial scale. Different process flow diagrams (PFDs) were compared, involving low (CaO storage at 50 °C) and high (800 °C) temperatures. The analysis is constructed upon the multicycle CaO conversion data reported in the previous section (Table 3). The multicycle CaO conversion was assumed to remain constant, as in cycle 20. Considering the operation of the plant, if the conversion eventually dropped below that level, it could be compensated by introducing a fraction of fresh material (makeup). Furthermore, it was assumed that there is no significant change in multicycle CaO conversion by increasing or decreasing the storage time, as indicated in Section 3.2.

The temperature in the solid storage vessels constrains the configuration of the process scheme and the efficiency since a more complex heat exchanger network is required in cases with low-temperature solid storage. Table 5 resumes the main assumptions for the CSP CaL schemes at low-temperature and high-temperature storage, which are taken from refs 13 and 15. Figure 8 shows a conceptual representation of these process schemes. Complete information about assumptions and process modeling can be found in the referenced papers since, for the comparison, the original configuration of the PFD is faithfully followed. Low-temperature storage allows energy storage without thermal losses (even in seasonal energy storage). Because of the high temperatures in both the calciner

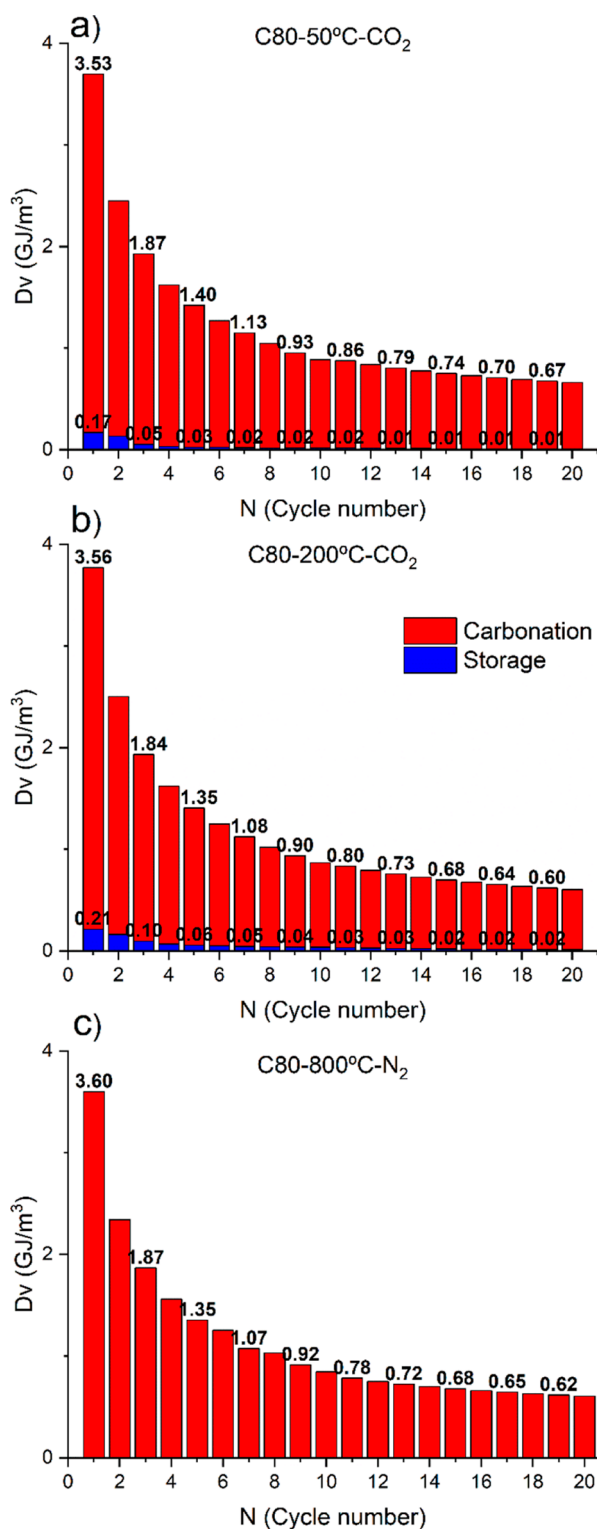


Figure 7. Volumetric energy density values as a function of the cycle number for C80 particles tested by including in the multicycle experiment a storage step at (a) 50 and (b) 200 °C in CO₂ and (c) 800 °C in N₂. Values were calculated using eq 7.

and the carbonator reactors, low-temperature storage involves a significant drop in the temperature of the materials throughout the cycle. It requires an optimized heat integration to achieve adequate system efficiency. When high-temperature solid storage is considered, the process scheme is simplified by requiring fewer heat exchangers because of a lower temper-

ature difference between the reactors and the storage. However, thermal losses increase at high temperatures, as well as problems related to the material's high-temperature cohesion.⁵⁸ This is not a minor matter as the increase in cohesiveness in the material as the temperature increases⁵⁹ would negatively affect the fluidization of the material to extract it from the storage tank to complete the carbonation cycle. To improve this situation, some coatings, such as silica or titania, could be added to the particles to improve their flowability.⁶⁰ From a life cycle and environmental assessment perspective, there are no significant differences between the storage of solids at high or low temperatures.⁴³

Given the advantages and disadvantages of storing solids at high temperatures, the cycle performance analysis provides valuable information for the overall process design.

Both PFDs were designed and simulated under steady-state conditions. The different PFDs (Figure 8) were modeled from the process scheme and the assumptions indicated in each reference work. Solar side losses were not considered for comparison since all the schemes are based on the same particle receiver size and temperature. Thus, the net thermal-to-electric efficiency was compared for each case. As is typical in many previous studies,² this efficiency was calculated as a weighted average throughout the day, assuming 8 h of constant solar irradiation in the “sun mode” and 16 h without radiation in the “night mode”. This involves a solar multiple (SM) of 3, with the SM being the receiver design thermal output ratio to the power block design thermal input. Under this simplified approach, the efficiency of the plant was calculated according to eq 8.¹⁹

$$\eta = \frac{\int_{24 \text{ h}} \dot{W}_{\text{net}} dt}{\int_{24 \text{ h}} \dot{Q}_{\text{input}} dt} = \frac{\dot{W}_{\text{net,sun}} \Delta t_{\text{sun}} + \dot{W}_{\text{net,night}} (24 - \Delta t_{\text{sun}})}{\dot{Q}_{\text{input}} \Delta t_{\text{sun}}} \quad (8)$$

where $\dot{W}_{\text{net,sun}}$ and $\dot{W}_{\text{net,night}}$ are the net power produced in “sun” and “night” modes, respectively, $\Delta t_{\text{sun}} = 18$ h, and \dot{Q}_{input} is the net solar power entering the power plant.

Equation 9 has been proposed to describe the overall energy storage capacity of the system to provide a more realistic measure of the energy density of the overall storage system.¹⁵ It is closely related to plant expenses and is a critical factor for accounting for the size of the vessels needed for both gas and solid storage. Reactors or heat exchangers are not included in the volumetric energy storage density since it is considered only the energy storage stage. Sensible heat stored accounts for around 40% of the high-temperature storage scheme (Figure 8b).

$$E_{\text{den}} = \frac{X \cdot (\Delta H_R + \int_{T_{\text{B,vessel}}}^{T_{\text{reactor}}} c_{p,B} dT + \int_{T_{\text{AB,vessel}}}^{T_{\text{A,vessel}}} c_{p,AB} dT) + (1 - X) \cdot \int_{T_{\text{AB,vessel}}}^{T_{\text{A,vessel}}} c_{p,A} dT}{\left(\frac{v_{\text{AB}}}{(1 - \epsilon_{\text{AB}})} + \frac{v_{\text{A}}}{(1 - \epsilon_{\text{A}})} \right) \cdot \frac{1}{\phi} + X \cdot v_{\text{B}}} \quad (9)$$

where X is the conversion, ΔH_R is the reaction enthalpy (GJ/kmol), $c_{p,i}$ is the specific heat of component i (MJ/kmol·K), T_{reactor} is the decomposition reaction temperature (K), $T_{i,\text{vessel}}$ is the storage temperature of component i (K), v_i is the specific volume of component i at storage conditions (m³/kmol), ϵ_i is the internal porosity of component i , and ϕ is the particle

Table 4. Accumulated Volumetric Energy Density of Limestone Samples with a Storage Step at 200 and 50 °C in CO₂ and 800 °C in an Inert Atmosphere (N₂)

sample	D_v (GJ/m ³)					
	storage 200 °C (CO ₂)		storage 50 °C (CO ₂)		storage 800 °C (N ₂)	
	carbonation	storage	carbonation	storage	carbonation	storage
C80	22.28	1.28	23.36	0.62	22.65	
C150	20.47	1.34	22.01	0.67	22.20	

Table 5. Main Assumptions in the CSP CaL Model

group	parameter	component	value
turbomachinery	isentropic efficiency	compressors, turbines	0.89
	number of intercooling/reheating stages	high pressure storage compressor (HPS-COMP)	5
		main CO ₂ compressor (M-COMP)	3
		CO ₂ turbine (HPS-TURB)	3
	intercooling/reheating temperature	high pressure storage compressor (HPS-COMP)	40 °C
		high pressure storage turbine (HPS-TURB)	65 °C/100 °C
heat exchangers	minimum temperature difference	gas–gas HX	15 °C
		solid–gas HX	15 °C
		solid–solid HX	20 °C
		CO ₂ cooler	20 °C
		coolers	1%
	pressure drops	HXG (both sides)	5%
		HRSG (hot side)	3%
		HRSG (cold side)	11%
		solid–gas HX (both sides)	3%
reactors	efficiency	calciner	1
	heat input	calciner	100 MW
	heat losses	carbonator	1% of heat transferred
storage vessels	temperature losses	all	0 °C
	CO ₂ storage conditions	CO ₂ vessel	75 bar 25 °C
steam cycle	isentropic efficiency	steam turbine (ST)	0.75
	mechanical–electric efficiencies	steam turbine (ST)	0.98
	condensing pressure	COND	0.075 bar
	evaporation pressure	HRSG	45 bar
	superheated steam temperature	HRSG	400 °C
heat rejection	auxiliaries electric power consumption	all coolers	0.8% of heat released

packing density, whose value is set to 0.6 as a standard value for the random loose packing fraction of irregularly shaped particles under gravity.

The experimental results (Table 3) show that multicycle CaO conversion does not vary significantly within the 80–150 μm particle size. Regarding temperature, CaO conversion slightly increases when considering low-temperature (and prolonged) solids storage. Figure 9a illustrates the net thermal-to-electric efficiency for the two particle sizes of solids and storage temperatures. By a comparison of the effect of the temperature on the thermal-to-electric efficiency, it can be seen that higher efficiency is achieved at higher storage temperatures. High-temperature storage implies a more straightforward and efficient energy integration process. In any case, the difference in the overall performance for each analyzed case is slight (+2–4%), reinforcing the finding that the system suffers a smooth penalty when storing the material at low temperature (allowing the energy storage in the long term) if adequate energy integration is carried out.

In addition to storing energy in the long term with a reduced energy penalty, storing solids at low temperatures presents a fundamental advantage regarding the flowability of the material. According to ref 58, when increasing the material

storage temperature from 25 to 500 °C at a consolidation stress of 1500 Pa, the tensile strength increases from around 50 Pa to above 700 Pa, directly impacting the material flowability. Hourly term storage temperatures higher than 500 °C would involve reaching the behavior of a very cohesive and nonflowing solid,⁵⁹ highly penalizing the process operation.

Regarding the overall energy density (Figure 9b) estimated by eq 9, the value is highly enhanced for high temperature due to the increase in sensible energy storage. Since the CaO conversions for high- and low-temperature storage are similar, there is not much impact associated with the number of solids to be stored (which penalizes the overall energy density). It is important to note that for calculating the required solid storage volume, the packing factor has been considered independent of the temperature (a constant value of 0.6⁶¹). However, the lab-scale test showed that the packing density smoothly increases with the temperature.⁵⁹

CONCLUSIONS

This work assesses the influence of the implementation of a storage phase on the multicycle performance of CaCO₃ with different PSDs. The innovation of the study resides in the consecution of the main objective: evaluate the influence of

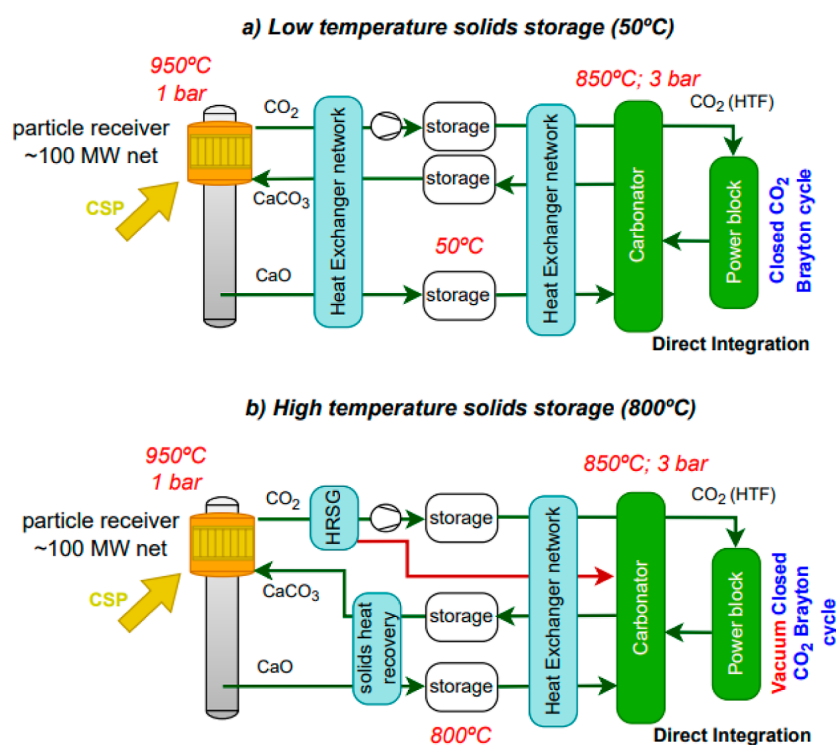


Figure 8. PFDs evaluated: (a) storage at low temperature (based on ref 13) and (b) storage at high temperature (based on ref 15).

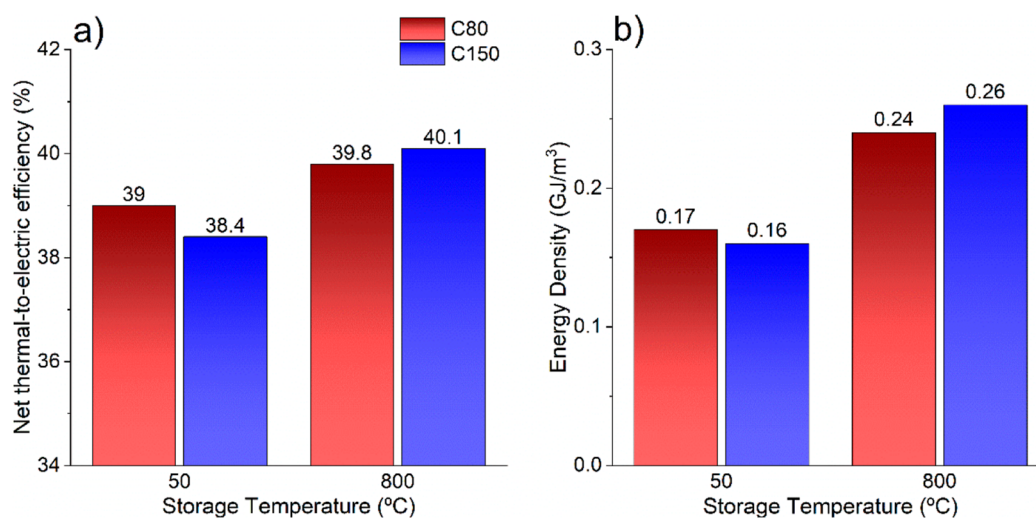


Figure 9. (a) Plant efficiency and (b) overall energy density as a function of the storage temperature and the particle size.

temperature, atmosphere, time, and particle size during the storage step. This allows for the assessment of the long-term energy storage performance, one of the key advantages of thermochemical energy storage systems.

Limestone particles of particle sizes in the range of 80–150 μm were tested for multicycle performance using schemes implementing a storage phase. Three different storage conditions were tested: 200 °C matching molten salts, 50 °C as room temperature in a CO_2 atmosphere, and 800 °C for industrial plant integration in N_2 . Results show that storage temperatures below 200 °C in CO_2 result in very slight residual carbonation and are mostly limited to the first few cycles. Thereafter, the decay in reactivity due to the progressive sintering of the material protects the cycled CaO to react significantly during the storage phase. Storage time does not

significantly impact the residual carbonation as it mostly occurs the first 5–10 min after CO_2 injection. For longer periods, the loss of active material becomes negligible. Thus, long-term storage at low temperatures appears to be viable even in a reactive atmosphere such as CO_2 .

For effective CaO conversion, the best performance was obtained for the C80 sample at a low-temperature storage step (at 50 °C, $X_{\text{CaO},20} = 0.126$). However, the difference with the other conditions tested are slight, thereby leading to the conclusion that there is limited dependence of conversion on the storage step.

From a process engineering perspective, storing solids at low temperatures can significantly improve their flowability, which could have a crucial effect on the overall process operation. Although a higher storage temperature facilitates energy

integration and system efficiency, the analysis results show that the effect of storing solids at ambient temperature is only 2–4% less as compared with that at high temperature. These results confirm the potential of the CaL process as a storage system in the long term. The lower energy density of the system when storing at low temperatures (losing the contribution of storing sensible heat) could be compensated by introducing a certain fraction of limestone makeup to enhance the average multicyclic conversion, which would considerably improve the energy storage density.

The results obtained are of utmost importance because the CaL system's main advantage is the possibility of storing the products of the reaction in the long term. Understanding this stage is fundamental for a profound knowledge of the CaL TCES system. Moreover, the results presented in this work could help in the development of more realistic engineering models.

AUTHOR INFORMATION

Corresponding Authors

Pedro E. Sánchez-Jiménez – Instituto de Ciencia de Materiales de Sevilla (C.S.I.C.-Universidad de Sevilla), Sevilla 41092, Spain; Departamento de Química Inorgánica, Facultad de Química, Universidad de Sevilla, Sevilla 41012, Spain; orcid.org/0000-0001-6982-1411; Email: aperejon@us.es

Luis A. Pérez Maqueda – Instituto de Ciencia de Materiales de Sevilla (C.S.I.C.-Universidad de Sevilla), Sevilla 41092, Spain; Email: maqueda@cica.es

Antonio Perejón – Instituto de Ciencia de Materiales de Sevilla (C.S.I.C.-Universidad de Sevilla), Sevilla 41092, Spain; Departamento de Química Inorgánica, Facultad de Química, Universidad de Sevilla, Sevilla 41012, Spain; orcid.org/0000-0002-5525-2227; Email: pedro.enrique@icmse.csic.es

Authors

Nabil Amghar – Instituto de Ciencia de Materiales de Sevilla (C.S.I.C.-Universidad de Sevilla), Sevilla 41092, Spain; orcid.org/0000-0002-0964-9899

Carlos Ortiz – Materials and Sustainability Group, Department of Engineering, Universidad Loyola Andalucía, Dos Hermanas 41704 Seville, Spain

Complete contact information is available at: <https://pubs.acs.org/10.1021/acs.energyfuels.3c02652>

Notes

The authors declare no competing financial interest.

ACKNOWLEDGMENTS

This work has been funded by the grant TED2021-131839B-C22 (Ministerio de Ciencia e Innovación). Financial support from project PDC2021-121552-C21 (MCIN/AEI/10.13039/501100011033 and European Union Next Generation EU/PRTR) is also acknowledged. N. Amghar acknowledges the PhD Fellowship grant PRE2018-085866 from the Spanish Government Agency Ministerio de Ciencia, Innovación y Universidades.

REFERENCES

- (1) Sarrion, B.; Valverde, J. M.; Perejon, A.; Perez-Maqueda, L.; Sanchez-Jimenez, P. E. On the Multicycle Activity of Natural Limestone/Dolomite for Thermochemical Energy Storage of Concentrated Solar Power. *Energy Technol.* **2016**, *4* (8), 1013–1019.
- (2) Ortiz, C.; Valverde, J. M.; Chacartegui, R.; Perez-Maqueda, L. A.; Giménez, P. The Calcium-Looping (CaCO₃/CaO) Process for Thermochemical Energy Storage in Concentrating Solar Power Plants. *Renewable Sustainable Energy Rev.* **2019**, *113* (July), 109252.
- (3) Sakellariou, K. G.; Karagiannakis, G.; Criado, Y. A.; Konstandopoulos, A. G. Calcium Oxide Based Materials for Thermochemical Heat Storage in Concentrated Solar Power Plants. *Sol. Energy* **2015**, *122*, 215–230.
- (4) Khan, M. I.; Asfand, F.; Al-Ghamdi, S. G. Progress in Research and Technological Advancements of Thermal Energy Storage Systems for Concentrated Solar Power. *J. Energy Storage* **2022**, *55* (PD), 105860.
- (5) Boot-Handford, M. E.; Abanades, J. C.; Anthony, E. J.; Blunt, M. J.; Brandani, S.; Mac Dowell, N.; Fernández, J. R.; Ferrari, M. C.; Gross, R.; Hallett, J. P.; et al. Carbon Capture and Storage Update. *Energy Environ. Sci.* **2014**, *7* (1), 130–189.
- (6) Kearns, D.; Liu, H.; Consoli, C. *Technology Readiness and Costs of CCS—Global CCS Institute*; Global CCS Institute, March, 2021; p 50.
- (7) Perejón, A.; Valverde, J. M.; Miranda-Pizarro, J.; Sánchez-Jiménez, P. E.; Pérez-Maqueda, L. A. Large-Scale Storage of Concentrated Solar Power from Industrial Waste. *ACS Sustain. Chem. Eng.* **2017**, *5* (3), 2265–2272.
- (8) Moreno, V.; Arcenegui-Troya, J.; Enrique Sánchez-Jiménez, P.; Perejón, A.; Chacartegui, R.; Manuel Valverde, J.; Allan Pérez-Maqueda, L. Albero: An Alternative Natural Material for Solar Energy Storage by the Calcium-Looping Process. *Chem. Eng. J.* **2022**, *440* (September 2021), 135707.
- (9) Gao, C.; Zhang, Y.; Li, D.; Li, M. Highly Cyclic Stability and Absorbent Activity of Carbide Slag Doped with MgO and ZnO for Thermochemical Energy Storage. *ACS Omega* **2022**, *7* (49), 45443–45454.
- (10) Raganati, F.; Ammendola, P. Review of Carbonate-Based Systems for Thermochemical Energy Storage for Concentrating Solar Power Applications: State-of-the-Art and Outlook. *Energy Fuels* **2023**, *37* (3), 1777–1808.
- (11) Liu, M.; Steven Tay, N.; Bell, S.; Belusko, M.; Jacob, R.; Will, G.; Saman, W.; Bruno, F. Review on Concentrating Solar Power Plants and New Developments in High Temperature Thermal Energy Storage Technologies. *Renewable Sustainable Energy Rev.* **2016**, *53*, 1411–1432.
- (12) Pelay, U.; Luo, L.; Fan, Y.; Stitou, D.; Rood, M. Thermal Energy Storage Systems for Concentrated Solar Power Plants. *Renewable Sustainable Energy Rev.* **2017**, *79*, 82–100.
- (13) Chacartegui, R.; Alovio, A.; Ortiz, C.; Valverde, J. M.; Verda, V.; Becerra, J. A. Thermochemical Energy Storage of Concentrated Solar Power by Integration of the Calcium Looping Process and a CO₂power Cycle. *Appl. Energy* **2016**, *173*, 589–605.
- (14) Ortiz, C.; Valverde, J. M.; Chacartegui, R.; Perez-Maqueda, L. A. Carbonation of Limestone Derived CaO for Thermochemical Energy Storage: From Kinetics to Process Integration in Concentrating Solar Plants. *ACS Sustain. Chem. Eng.* **2018**, *6* (5), 6404–6417.
- (15) Ortiz, C.; Romano, M. C.; Valverde, J. M.; Binotti, M.; Chacartegui, R. Process Integration of Calcium-Looping Thermochemical Energy Storage System in Concentrating Solar Power Plants. *Energy* **2018**, *155*, 535–551.
- (16) Barin, I. *Thermochemical Data of Pure Substances*; Wiley, 1995.
- (17) Sarrion, B.; Perejón, A.; Sánchez-Jiménez, P. E.; Pérez-Maqueda, L. A.; Valverde, J. M. Role of Calcium Looping Conditions on the Performance of Natural and Synthetic Ca-Based Materials for Energy Storage. *J. CO₂ Util.* **2018**, *28* (October), 374–384.
- (18) Sarrion, B.; Sanchez-Jimenez, P. E.; Perejon, A.; Perez-Maqueda, L. A.; Valverde, J. M. Pressure Effect on the Multicycle Activity of Natural Carbonates and a Ca/Zr Composite for Energy Storage of Concentrated Solar Power. *ACS Sustain. Chem. Eng.* **2018**, *6* (6), 7849–7858.

- (19) Alovio, A.; Chacartegui, R.; Ortiz, C.; Valverde, J. M.; Verda, V. Optimizing the CSP-Calcium Looping Integration for Thermochemical Energy Storage. *Energy Convers. Manag.* **2017**, *136*, 85–98.
- (20) Arcenogui Troya, J. J.; Moreno, V.; Sanchez-Jiménez, P. E.; Perejón, A.; Valverde, J. M.; Pérez-Maqueda, L. A. Effect of Steam Injection during Carbonation on the Multicyclic Performance of Limestone (CaCO₃) under Different Calcium Looping Conditions: A Comparative Study. *ACS Sustain. Chem. Eng.* **2022**, *10* (2), 850–859.
- (21) Valverde, J. M.; Sanchez-Jimenez, P. E.; Perez-Maqueda, L. A.; Quintanilla, M. A. S.; Perez-Vaquero, J. Role of Crystal Structure on CO₂ Capture by Limestone Derived CaO Subjected to Carbonation/Recarbonation/Calcination Cycles at Ca-Looping Conditions. *Appl. Energy* **2014**, *125*, 264–275.
- (22) Borgwardt, R. H. Calcium Oxide Sintering in Atmospheres Containing Water and Carbon Dioxide. *Ind. Eng. Chem. Res.* **1989**, *28* (4), 493–500.
- (23) Scaltsoyiannes, A. A.; Lemonidou, A. A. On the Factors Affecting the Deactivation of Limestone under Calcium Looping Conditions: A New Comprehensive Model. *Chem. Eng. Sci.* **2021**, *243*, 116797.
- (24) Sarrión, B.; Perejón, A.; Sánchez-Jiménez, P. E.; Amghar, N.; Chacartegui, R.; Manuel Valverde, J.; Pérez-Maqueda, L. A. Calcination under Low CO₂ Pressure Enhances the Calcium Looping Performance of Limestone for Thermochemical Energy Storage. *Chem. Eng. J.* **2021**, *417* (September 2020), 127922.
- (25) Manovic, V.; Charland, J. P.; Blamey, J.; Fennell, P. S.; Lu, D. Y.; Anthony, E. J. Influence of Calcination Conditions on Carrying Capacity of CaO-Based Sorbent in CO₂ Looping Cycles. *Fuel* **2009**, *88* (10), 1893–1900.
- (26) Valverde, J. M.; Medina, S. Reduction of Calcination Temperature in the Calcium Looping Process for CO₂ Capture by Using Helium: In Situ XRD Analysis. *ACS Sustain. Chem. Eng.* **2016**, *4* (12), 7090–7097.
- (27) Bayon, A.; Bader, R.; Jafarian, M.; Fedunik-Hofman, L.; Sun, Y.; Hinkley, J.; Miller, S.; Lipiński, W. Techno-Economic Assessment of Solid-Gas Thermochemical Energy Storage Systems for Solar Thermal Power Applications. *Energy* **2018**, *149*, 473–484.
- (28) Hanak, D. P.; Manovic, V. Economic Feasibility of Calcium Looping under Uncertainty. *Appl. Energy* **2017**, *208* (September), 691–702.
- (29) Da, Y.; Xuan, Y.; Teng, L.; Zhang, K.; Liu, X.; Ding, Y. Calcium-Based Composites for Direct Solar-Thermal Conversion and Thermochemical Energy Storage. *Chem. Eng. J.* **2020**, *382* (June 2019), 122815.
- (30) Ho, C. K. A Review of High-Temperature Particle Receivers for Concentrating Solar Power. *Appl. Therm. Eng.* **2016**, *109*, 958–969.
- (31) Ortiz, C.; Valverde, J. M.; Chacartegui, R.; Romeo, L. M.; Perez-Maqueda, L. A. The MOxy-CaL Process: Integration of Membrane Separation, Partial Oxy-Combustion and Calcium Looping for CO₂ Capture. *Chem. Eng. Trans.* **2018**, *70*, 643–648.
- (32) Hanak, D. P.; Manovic, V. Calcium Looping with Supercritical CO₂ Cycle for Decarbonisation of Coal-Fired Power Plant. *Energy* **2016**, *102*, 343–353.
- (33) Martínez, A.; Lara, Y.; Lisbona, P.; Romeo, L. M. Energy Penalty Reduction in the Calcium Looping Cycle. *Int. J. Greenhouse Gas Control* **2012**, *7*, 74–81.
- (34) Vorrias, I.; Atonios, K.; Nikolopoulos, A.; Nikolopoulos, N.; Grammelis, P.; Kakaras, E. Calcium Looping for CO₂ Capture from a Lignite Fired Power Plant. *Fuel* **2013**, *113*, 826–836.
- (35) Arias, B.; Diego, M. E.; Abanades, J. C.; Lorenzo, M.; Diaz, L.; Martínez, D.; Alvarez, J.; Sánchez-Biezma, A. Demonstration of Steady State CO₂ Capture in a 1.7MWth Calcium Looping Pilot. *Int. J. Greenhouse Gas Control* **2013**, *18*, 237–245.
- (36) Tregambi, C.; Salatino, P.; Solimene, R.; Montagnaro, F. An Experimental Characterization of Calcium Looping Integrated with Concentrated Solar Power. *Chem. Eng. J.* **2018**, *331* (May 2017), 794–802.
- (37) Matthews, L.; Lipiński, W. Thermodynamic Analysis of Solar Thermochemical CO₂ Capture via Carbonation/Calcination Cycle with Heat Recovery. *Energy* **2012**, *45* (1), 900–907.
- (38) Chen, X.; Jin, X.; Ling, X.; Wang, Y. Exergy Analysis of Concentrated Solar Power Plants with Thermochemical Energy Storage Based on Calcium Looping. *ACS Sustain. Chem. Eng.* **2020**, *8* (21), 7928–7941.
- (39) Palacios, A.; Barreneche, C.; Navarro, M. E.; Ding, Y. Thermal Energy Storage Technologies for Concentrated Solar Power - A Review from a Materials Perspective. *Renewable Energy* **2020**, *156*, 1244–1265.
- (40) Ortiz, C.; Chacartegui, R.; Valverde, J. M.; Carro, A.; Tejada, C.; Valverde, J. Increasing the Solar Share in Combined Cycles through Thermochemical Energy Storage. *Energy Convers. Manag.* **2021**, *229* (November2020), 113730.
- (41) Karasavvas, E.; Panopoulos, K. D.; Papadopoulou, S.; Voutetakis, S. Energy and Exergy Analysis of the Integration of Concentrated Solar Power with Calcium Looping for Power Production and Thermochemical Energy Storage. *Renewable Energy* **2020**, *154*, 743–753.
- (42) Pascual, S.; Lisbona, P.; Romeo, L. M. Operation Maps in Calcium Looping Thermochemical Energy Storage for Concentrating Solar Power Plants. *J. Energy Storage* **2022**, *55* (PD), 105771.
- (43) Colelli, G.; Chacartegui, R.; Ortiz, C.; Carro, A.; Arena, A. P.; Verda, V. Life Cycle and Environmental Assessment of Calcium Looping (CaL) in Solar Thermochemical Energy Storage. *Energy Convers. Manag.* **2022**, *257* (December 2021), 115428.
- (44) Tesio, U.; Guelpa, E.; Verda, V. Integration of Thermochemical Energy Storage in Concentrated Solar Power. Part 1: Energy and Economic Analysis/Optimization. *Energy Convers. Manage.: X* **2020**, *6* (March), 100039.
- (45) Pelay, U.; Luo, L.; Fan, Y.; Stitou, D.; Castelain, C. Integration of a Thermochemical Energy Storage System in a Rankine Cycle Driven by Concentrating Solar Power: Energy and Exergy Analyses. *Energy* **2019**, *167*, 498–510.
- (46) Cannone, S. F.; Stendardo, S.; Lanzini, A. Solar-Powered Rankine Cycle Assisted by an Innovative Calcium Looping Process as an Energy Storage System. *Ind. Eng. Chem. Res.* **2020**, *59* (15), 6977–6993.
- (47) Amghar, N.; Ortiz, C.; Perejón, A.; Valverde, J. M.; Maqueda, L. P.; Sánchez Jiménez, P. E. The SrCO₃/SrO System for Thermochemical Energy Storage at Ultra-High Temperature. *Sol. Energy Mater. Sol. Cells* **2022**, *238*, 111632.
- (48) Ortiz, C.; Valverde, J. M.; Chacartegui, R.; Pérez-Maqueda, L. A.; Gimenez-gavarrell, P. Scaling-up the Calcium-Looping Process for CO₂ Capture and Energy Storage. *KONA Powder Part. J.* **2021**, *38* (0), 189–208.
- (49) Hanak, D. P.; Anthony, E. J.; Manovic, V. A Review of Developments in Pilot-Plant Testing and Modelling of Calcium Looping Process for CO₂ Capture from Power Generation Systems. *Energy Environ. Sci.* **2015**, *8* (8), 2199–2249.
- (50) Abanades, J. C.; Alvarez, D. Conversion Limits in the Reaction of CO₂ with Lime. *Energy Fuels* **2003**, *17* (2), 308–315.
- (51) Espin, M. J.; Duran-Olivencia, F. J.; Valverde, J. M. Role of Particle Size on the Cohesive Behavior of Limestone Powders at High Temperature. *Chem. Eng. J.* **2020**, *391* (September 2019), 123520.
- (52) Valverde, J. M.; Sanchez-Jimenez, P. E.; Perejon, A.; Perez-Maqueda, L. A. CO₂Multicyclic Capture of Pretreated/Doped CaO in the Ca-Looping Process. Theory and Experiments. *Phys. Chem. Chem. Phys.* **2013**, *15* (28), 11775–11793.
- (53) Fedunik-Hofman, L.; Bayon, A.; Donne, S. W. Kinetics of Solid-Gas Reactions and Their Application to Carbonate Looping Systems. *Energies* **2019**, *12* (15), 2981.
- (54) Blamey, J.; Anthony, E. J.; Wang, J.; Fennell, P. S. The Calcium Looping Cycle for Large-Scale CO₂ Capture. *Prog. Energy Combust. Sci.* **2010**, *36* (2), 260–279.
- (55) Valverde, J. M.; Sanchez-Jimenez, P. E.; Perez-Maqueda, L. A. Role of Precalcination and Regeneration Conditions on Postcombustion

tion CO₂ Capture in the Ca-Looping Technology. *Appl. Energy* **2014**, *136*, 347–356.

(56) Alva, G.; Lin, Y.; Fang, G. An Overview of Thermal Energy Storage Systems. *Energy* **2018**, *144*, 341–378.

(57) Durán-Martín, J. D.; Sánchez Jimenez, P. E.; Valverde, J. M.; Perejón, A.; Arcenegui-Troya, J.; García Triñanes, P.; Pérez Maqueda, L. A. Role of Particle Size on the Multicycle Calcium Looping Activity of Limestone for Thermochemical Energy Storage. *J. Adv. Res.* **2020**, *22*, 67–76.

(58) Durán-Olivencia, F.; Espín, M.; Valverde, J. M. Cross Effect between Temperature and Consolidation on the Flow Behavior of Granular Materials in Thermal Energy Storage Systems. *Powder Technol.* **2020**, *363*, 135–145.

(59) Durán-Olivencia, F.; Ebri, J. M. P.; Espín, M.; Valverde, J. M. The Cohesive Behavior of Granular Solids at High Temperature in Solar Energy Storage. *Energy Convers. Manag.* **2021**, *240* (November 2020), 114217.

(60) Gannoun, R.; Durán-Olivencia, F.; Pérez, A.; Valverde, J. M. Titania Coatings: A Mechanical Shield for Cohesive Granular Media at High Temperatures. *Chem. Eng. J.* **2022**, *450* (P3), 138123.

(61) Valverde, J. M.; Castellanos, A. Random Loose Packing of Cohesive Granular Materials. *Europhys. Lett.* **2006**, *75* (6), 985–991.